Available online at www.sciencedirect.com
ScienceDirect
Journal of Power Sources 160 (2006) 602–608
JOURNAL OF POWER SOURCES
www.elsevier.com/locate/jpowsour

Cycle-life testing of 100-Ah class lithium-ion battery in a simulated geosynchronous-Earth-orbit satellite operation

Xianming Wang *, Yoshitsugu Sone, Hitoshi Naito, Chisa Yamada, Go Segami, Koichi Kibe

Institute of Aerospace Technology, Japan Aerospace Exploration Agency, Tsukuba Space Center, Sengen 2-1-1, Ibaraki 305-8505, Japan

Received 7 October 2005; received in revised form 7 January 2006; accepted 14 January 2006
Available online 23 February 2006

Abstract

In this paper, we review our work on cycle-life testing of a 100-Ah class lithium-ion battery in a simulated geosynchronous-Earth-orbit (GEO) satellite operation. The battery consists of ten 100-Ah lithium-ion (10) cells in a series, with a high energy density exceeding 100 Wh kg^{-1} at the battery level. We simulate the eclipse period in real-time testing with five depth-of-discharge (DOD) patterns at an ambient temperature of 15 °C. We also simulate a sun-shine period in 8-day thermally accelerated full-charge storage at an ambient temperature of 25 °C, which in our experience corresponds to full-charge storage of a half-year operation at 0 °C. Eighteen eclipse seasons have presently been completed, corresponding to 9 years of GEO operation. The battery maintained a high voltage near 3.4 V at the end of the discharge, even when the DOD was set at 70%. The voltage dispersion of 10 cells was also sufficiently small in the range of 48 mV. The cell temperature reached a maximum of 29 °C and maintained minimal dispersion smaller than 4 °C even when the battery was discharged at a high DOD of 70%.

Keywords: Lithium-ion battery; Cycle-life testing; Geosynchronous-Earth-orbit (GEO); Satellite

1. Introduction

The rechargeable battery system in a spacecraft performs energy storage and generation, and is generally one of the most massive components. Cost is a fundamental limitation to nearly all space missions, so it is very important to reduce the weight and size of the rechargeable battery to achieve the greatest return from a space investment. Lithium-ion batteries, which have a high energy density and high working voltage, are expected to replace conventional nickel–cadmium (Ni–Cd) and nickel–hydrogen (Ni–H_2) batteries.

To employ lithium-ion batteries in space applications, we must consider some particular operational conditions and environments, such as vacuum, out-gassing from the polymer components, safety concerns, long cycle-life requirements, and charge and discharge intervals limited strictly by the spacecraft orbit. For a satellite in geosynchronous-Earth-orbit (GEO, 36,000 km from the Earth), the rechargeable batteries are discharged in a maximum of 72 min to generate enough power to meet electrical demands of the bus and mission over a 45-day period on each side of the equinox of a year. At all other times, the GEO satellite is free from the Earth's shadow, and the solar cells charge the rechargeable batteries at an optimum state of charge (SOC). The typical cycle-life requirement for rechargeable batteries in a GEO satellite is 1350 cycles, corresponding to a 15-year mission. This makes it important to optimize the operation conditions, such as storage temperature, charge rate and taper voltage. For this reason, many rather novel experiment investigations need to be conducted in order to utilize lithium-ion batteries as power sources in space.

Lithium-ion cells with capacities ranging from 0.6 Ah to 100 Ah are being assessed in real-time by simulating low-Earth-orbit (LEO) and GEO satellite operations at the Japan Aerospace Exploration Agency (JAXA, formerly the National Space Development Agency of Japan) [1–3]. The cycle-life target is 30,000 cycles (5 years) for LEO operation and 1350 cycles (15 years) for GEO applications. A few types of these cells have exhibited impressive performance. Their energy densities exceed 100 Wh kg^{-1}, about twice those of Ni–Cd and Ni–H_2 cells. Furthermore, excellent cycle lives have been verified, exceeding 29,000 cycles in LEO simulation mode and 1700 cycles in GEO simulation mode with a cell voltage above 3.0 V at the end of

* Corresponding author. Tel.: +81 29 868 4247; fax: +81 29 868 5969.
E-mail address: oh.kenmei@jaxa.jp (X. Wang).

0378-7753/$ – see front matter © 2006 Elsevier B.V. All rights reserved.
doi:10.1016/j.jpowsour.2006.01.052

the discharge. The satisfactory on-ground evaluation results have encouraged us to apply the cycling performance of lithium-ion cells to a practical space environment. The same effort is also be undertaken by other space organizations [4–12]. It has been reported that more than 10 spacecraft with on-board lithium-ion batteries have been launched in recent years. The spacecraft include satellites, Mars rovers, and space vehicles, most of them operating in a LEO environment.

We began conducting cycle-life testing of 100-Ah class lithium-ion battery in simulated GEO operation in 2002. Mitsubishi Electric Corporation (MELCO) constructed the battery assembly using 10 in-series 100-Ah lithium-ion cells supplied by GS Yuasa Technology Ltd. (GYT, formerly Japan Storage Battery Co. Ltd.). Before the cycle-life testing, this battery underwent vibration, shock, and thermal vacuum qualification testing at MELCO. The previous report demonstrated the excellent endurance of this battery for the GEO space environment and for launch vibration [5,6]. Our goal in this work is to determine the cycle life of this battery in a real-time testing simulating the eclipse period and an 8-day thermally accelerated full-charge storage simulating the sun-shine period. This paper provides a review of the latest test results.

2. Experimental

2.1. Battery description

The battery consists of ten 100-Ah lithium-ion (10) cells in a series, developed specifically for space applications. We did not specially match the cells used in this battery in order to evaluate their performance dispersion. These cells were selected from a few tens of cells in the same lot and passed the shipping check criteria, including weight, size, capacity, ac impedance (1 kHz), and open-circuit voltage. Table 1 lists the typical cell specifications and battery features.

The lithium-ion cells have an elliptic cylindrical shape [7]. The conventional assembly approaches used for prismatic Ni–Cd batteries can be applied to these lithium-ion cells by assembling the cells side by side, providing an efficient packing configuration. Good heat radiation can also be realized due to wide planes on both sides. A lithium cobalt dioxide ($LiCoO_2$) cathode and a graphite anode are used in these cells, with a lithium salt dissolved in alkyl carbonate mixed solvent. The cell element is tightly enclosed in an aluminum-alloy container with rupture plates. The positive and negative terminals are hermetically sealed with a metal-brazed ceramic seal. The cells passed qualification testing under the most severe environmental conditions in the space program, including mechanical and safety items [7].

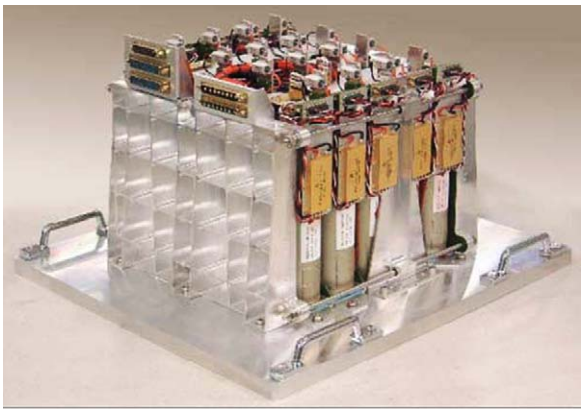

Fig. 1. Photograph of battery assembly with ten 100-Ah class lithium-ion cells.

A photograph of the battery is provided in Fig. 1. The battery has a high energy density that exceeds 100 Wh kg^{-1}. The shunt circuit protects the cells against overcharge in the event of abuse, and equalizes each cell voltage. The bypass switch is connected to every cell in parallel, and works only in the event of a single cell failure in open circuit. The function of the bypass switch is to provide a bypass for charge–discharge current in order to ensure normal operation of the other cells connected to the failing cell in series. Double insulation between the cell case and chassis protects the battery against electrical insulation failure. Due to the optimal thermal design, the battery exhibits superior heat dissipation with a design value of thermal gradient deviation smaller than 10 °C by considering the cell-temperature-dispersion increase at the end of the life. This battery had a qualification-test history before we began conducting the cycle-life testing.

Additional details can be found in other reports [4–8].

2.2. GEO simulation conditions

The battery is set in a thermostatic incubator with a control accuracy of 1 °C. The ambient temperature of the thermostatic incubator is remotely controlled by a thermal sensor near the battery. We monitor the cell voltage, battery voltage, current, cell temperature, and incubator temperature during the testing. Table 2 summarizes the charge–discharge conditions that simulate GEO operation.

The on-board battery is expected to maintain 0 °C with a SOC of 100% during a sun-shine period. The calendar life per-

Table 1
Cell specifications and battery features

	Capacity (Ah)		Voltage (V)	Mass (kg)	Dimensions (mm)			Energy density (Wh kg^{-1})
	Rated	Nominal[a]			Width	Length	Height	
Cell	100	110	3.7	2.8	50	130	208	145
Battery	100	–	37	35	328	275	352	106

[a] Charge: CC–CV, 20 A, 3.98 V, 8 h; discharge: CC, 50 A, 2.75 V; ambient temperature: 15 °C.

Table 2
Operation conditions of 100-Ah class lithium-ion battery

Phase	Ambient temperature (°C)	Condition	Status
Sun shine	25	Storage—8 days, full charge Pre-charge—CC–CV: 10 A (0.1 C), 39.5 V or 40.0 V, 23.3 h	18 eclipse seasons
Eclipse, 45 cycles	15	(1) Charge—CC–CV: 10 A (0.1 C), 39.5 V, 23.3 h Discharge—CC: 60 A (0.6 C), 40 min (40% DOD) 6 cycles	
		(2) Charge—CC–CV: 10 A (0.1 C), 39.5 V, 23 h Discharge—CC: 60 A (0.6 C), 60 min (60% DOD) 7 cycles	
		(3) Charge—CC–CV: 10 A (0.1 C), 39.5 V, 22.8 h Discharge—CC: 60 A (0.6 C), 70.5 min (70.5% DOD) 19 cycles	
		(4) Same as (2) (5) Same as (1) Taper voltage was changed from 39.5 V to 40.0 V from the 16th eclipse season since cell voltage at the end of the discharge declined to 3.3 V	
Capacity verification	15	Charge—CC–CV: 10 A (0.1 C), 39.5 V or 40.0 V, 16 h Discharge—CC: 50 A (0.5 C), 2.75 V cell^{-1}	

formance of this type of cell has been found to obey the following equation [13]:

$$Q_{\mathrm{cf}} = K_{\mathrm{f}} t^{1/2} + b \tag{1}$$

$$K_{\mathrm{f}} = \exp\left[\frac{14.769 - 4.5518 \times 1000}{273 + T}\right] \tag{2}$$

Here, Q_{cf} (%) is the capacity loss due to calendar storage, K_{f} the coefficient, t (day) the storage duration, b the constant, and T (K) is the absolute temperature. Based on this knowledge, we simulate a sun-shine period in 8-day thermally accelerated full-charge storage at an ambient temperature of 25 °C in this testing, which corresponds to full-charge storage of a half year at 0 °C.

We simulate the eclipse period in real-time testing with five depth-of-discharge (DOD) patterns. A 45-cycle charge–discharge is performed at an ambient temperature of 15 °C in each eclipse period. The battery is managed by a constant current–constant voltage (CC–CV) charge mode. The taper voltage was set at a low value of 39.5 V at the beginning of life (BOL) phase. We raised the taper voltage to 40.0 V to compensate the capacity loss when the cell voltage at the end of the discharge declines to 3.3 V. The maximum taper voltage is 41.0 V for GEO operation. We do not activate the balancing circuit so as to facilitate evaluating the voltage dispersion during charging and discharging for these 10 cells.

We measure the cell capacity at the beginning and end of the life testing at each taper voltage. Due to the connector-number limitation, the capacity verification is completed when the voltage of any one cell reaches the cut-off value (2.75 V), i.e. only the cell with the lowest discharge capacity can be measured.

3. Results and discussion

The battery has been tested for more than 810 cycles (18 eclipse seasons) as of June 30, 2005. The cell voltage at the end of the discharge declined to near 3.3 V at the maximum DOD of 70% in the 15th season. We raised the taper voltage from 39.5 V to 40.0 V from the 676th cycle (16th eclipse season) to increase the cell capacity.

Fig. 2 plots the initial capacity–check curves of 10 cells. We observed the typical voltage–capacity curve of the $LiCoO_2$ cathode and graphite anode. Cell no. 3 exhibits a lower voltage and smaller capacity than the other cells in the discharge phase.

Fig. 3 depicts the voltage trend of every cell at the end of the charge and discharge. Four conclusions can be drawn here. First, the cell voltage at the end of the discharge maintained a high level of near 3.4 V. Second, raising the taper voltage increased the cell voltage at the end of the discharge. This phenomenon was most

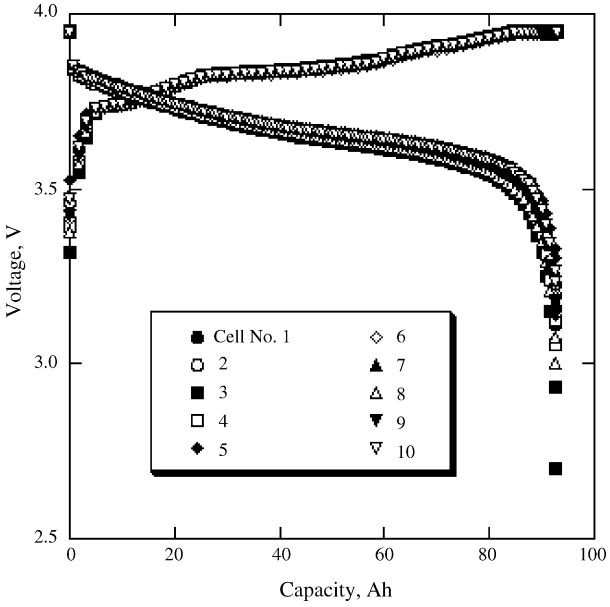

Fig. 2. Initial capacity–check curves.

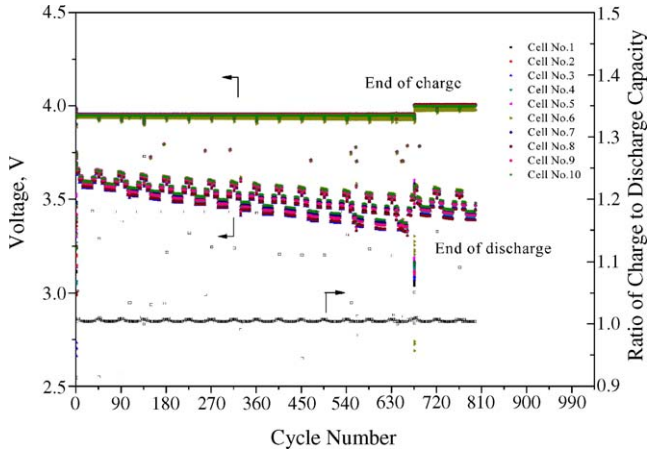

Fig. 3. Voltage trend at end of charge and discharge.

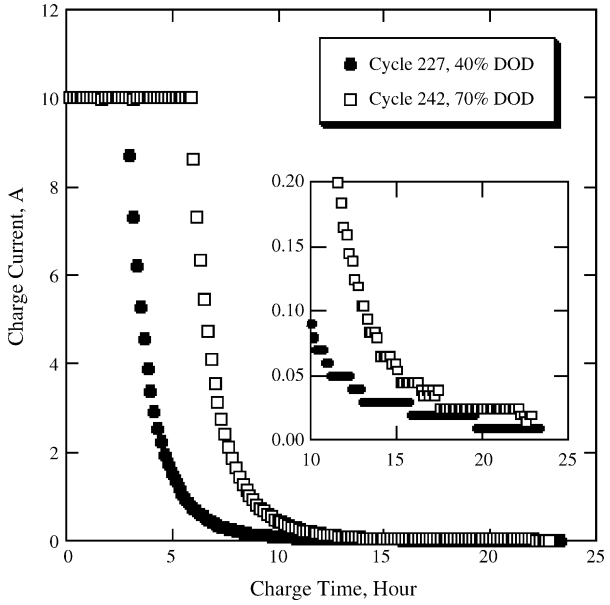

Fig. 4. Comparison of charge–current curves.

remarkable for a large DOD. Third, the cell voltage difference at 70% DOD and 40% DOD in the same season increased with cycling. This may be attributed to the cell-internal impedance increase during life testing. Another possible explanation for this phenomenon is the cell discharge characteristic with a large voltage slope at low SOC. This difference was suppressed after the taper voltage was raised, as observed in the 15th and 16th seasons. Fourth, the cell-voltage dispersion at the end of the charge and discharge was sufficiently small as a function of the cycle number and DOD. The maximum cell-voltage dispersion was 32 mV at the end of the charge and 48 mV at the end of the discharge in the 18th season. The cell-voltage dispersion appeared to have little dependence on increases in the taper voltage. However, the cell with the lowest discharge voltage was different before and after the taper voltage was increased, as seen in Fig. 5.

Fig. 3 also presents the ratio of the charge to the discharge capacity (*C*/*D* ratio) at each cycle, which reflects the capacity recovery during cycling. Overall, the *C*/*D* ratio was greater than 1.0, indicating good capacity recovery under the GEO-simulated conditions. Additionally, we note that the *C*/*D* ratio at the same DOD was almost independent of the cell number and taper voltage. Comparing the *C*/*D* ratio at different DODs discloses that the *C*/*D* ratio tended to be high at a small DOD. To clarify this issue, we investigate the charge–current curves of the 227th (40% DOD) and 242nd (70% DOD) cycles in Fig. 4. Obviously, the current at the end of the charge at the 242nd cycle exceeded that of the 227th cycle, indicating an insufficient charging after the discharge at a large DOD. The only difference in charge condition for these two cycles was the charge time, as shown in Table 2. We can therefore reasonably attribute the low *C*/*D* ratio at a large DOD to the short charge time.

We summarize the cell voltages at the end of some typical charge and discharge cycles with 70% DOD to clarify the above results (Fig. 5). The voltage at the end of the charge was obviously different for each cell. This phenomenon can be attributed to the different internal impedance values of these cells, which is commonly observed in cells connected in a series. Since the CC–CV charge of these cells is controlled by the total voltage, a cell with low internal impedance should have a low cell voltage at the end of the charge due to slight *iR*-drop effect. Here, the resistance increase reflects cell performance degradation. In GEO operation, the charge–discharge cycle results in both the reduction decomposition of electrolyte at the graphite

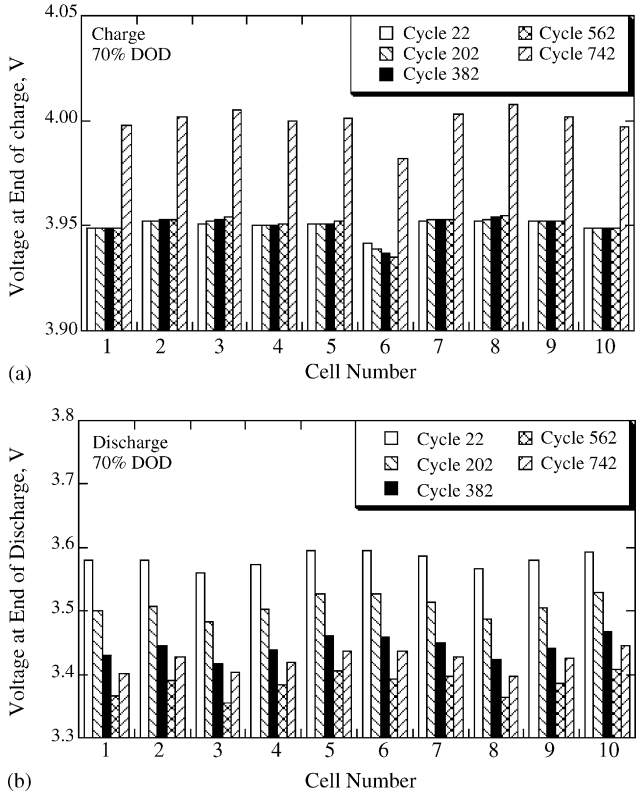

Fig. 5. Cell voltages at end of charge (a) and discharge (b) of some typical cycles with 70% DOD.

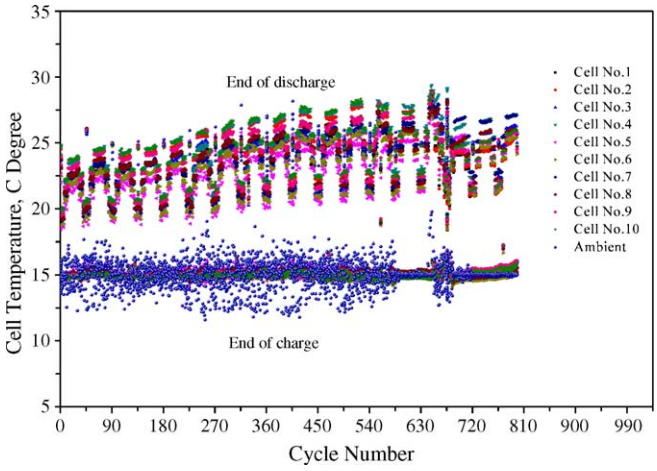

Fig. 6. Temperature trend at end of charge and discharge.

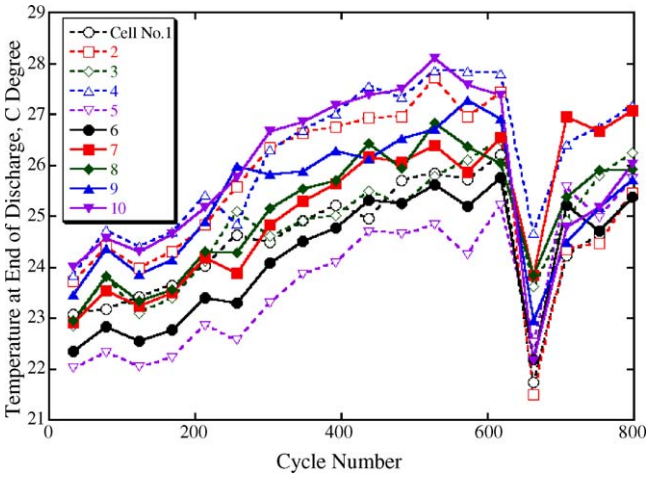

Fig. 8. Cell-temperature comparison at end of discharge.

surface and structure destruction of the $LiCoO_2$ cathode. These may be the primary causes of resistance increase with cycling. Based on this interpretation, we can deduce that cell no. 6 had a lower internal impedance than the other cells, and cell nos. 3 and 8 had substantial internal impedance. The cell with the lowest voltage at the end of the discharge was different before and after increasing the taper voltage. Cell no. 3 (no. 8) exhibited the poorest discharge behavior among the 10 cells at a taper voltage of 39.5 V (40.0 V). To a certain extent, this result supports the above deduction that cell nos. 3 and 8 had substantial internal impedance.

The temperature trend at the end of the charge and discharge is presented in Fig. 6. The temperature at the end of the charge remained near the setup value of 15 °C, independent of the cycle number and DOD. The temperature at the end of the discharge increased with the cycle number and DOD and had a maximum value of 29 °C in the 15th season (also see Fig. 7). Raising the taper voltage reduced the cell temperature at the end of the discharge. This may be attributed to the high cell SOC due to the cell charging at a high taper voltage. The cell-temperature dispersion increased with the cycle number and DOD, and had a maximum around 4 °C. The taper voltage increases appeared to have little effect on suppressing the cell-temperature dispersion, though the cell with the lowest temperature changed before and after the taper voltage was increased. After the 583rd cycle, we performed periodic maintenance of the thermostatic incubator. Consequently, the thermostatic capacity of the incubator was effectively improved in the sequence cycles.

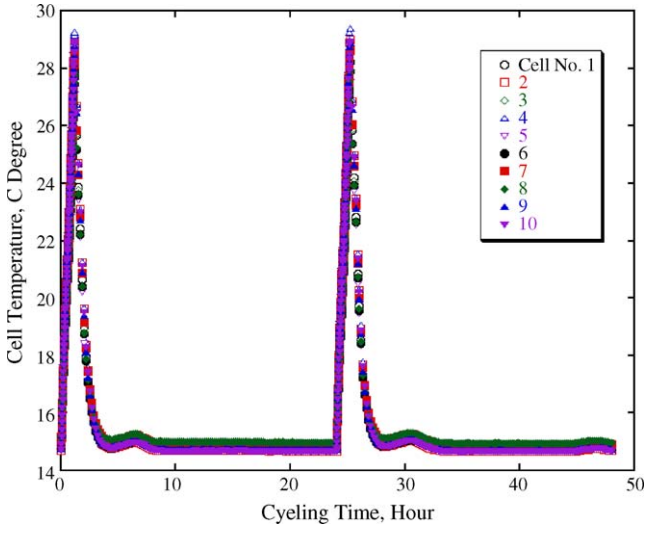

Fig. 7. Cell-temperature curves at cycles 648 and 649.

Fig. 8 compares the temperatures at the end of the discharge of the 10 cells with 70% DOD as a function of cycle number. The cell temperature at the end of the discharge changed before and after the taper voltage was raised. Cell nos. 5 and 6 (cell nos. 10 and 4) had the lowest (highest) temperature at the end of the discharge at a taper voltage of 39.5 V. The temperatures of cell nos. 1, 2, and 6 (cell nos. 7 and 4) became the lowest (highest) at the end of the discharge after the taper voltage was raised to 40.0 V. It is possible that the unbalanced distribution of ambient temperature in the thermostatic incubator, in addition to cell performance degradation, is also an important factor that results in cell temperature dispersion.

Fig. 9 presents the capacity-verification results at different taper voltages in terms of capacity retention. Cell no. 3 had the lowest capacity of 92 Ah among the 10 cells with a taper voltage of 39.5 V at the beginning of the life testing. An initial capacity lower than the nominal value is primarily due to the different charge–discharge conditions for these capacity-verification testing, as shown in Tables 1 and 2. The capacity of cell no. 6 became the lowest after 15 seasons and declined to 80 Ah, indicating relatively serious fading of cell no. 6 in discharge capacity due to prolonged cycling and storage conditions. A taper voltage increase from 39.5 V to 40.0 V effectively increased the capacity of cell no. 6 to 92 Ah.

There are a few possible explanations for the low discharge capacity of cell no. 6, including high internal impedance, low capacity due to cell-performance degradation, and charge capacity deficiency. We investigate the charge curves of capacity

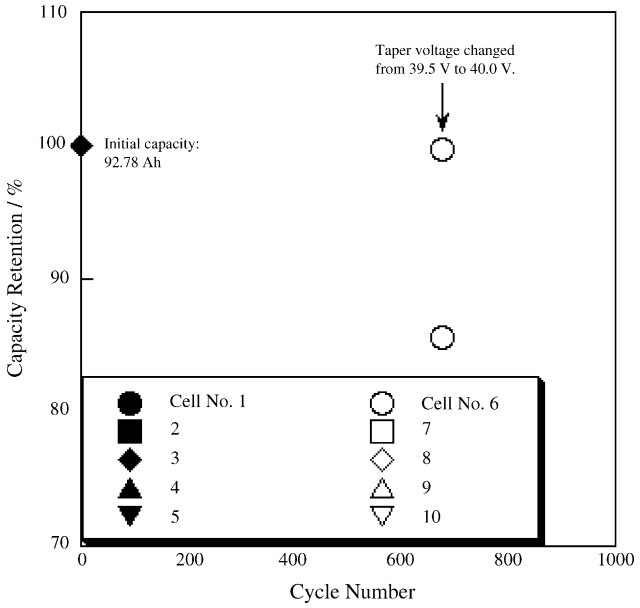

Fig. 9. Verification results of cell capacity.

verification at a taper voltage of 39.5 V to clarify this issue (Fig. 10). Obviously, the charge curve was different for each cell; cell no. 6 had the lowest upper voltage in both cases. Generally, the apparent cell voltage in the charge–discharge curve includes the real cell voltage and *iR*-drop. Since cell no. 6 (cell nos. 3 and 8) had smaller (larger) cell-internal impedance than the other cells, as described above, the *iR*-drop effect made cell 6 (cell nos. 3 and 8) exhibit a low (high) charge voltage. This tendency was maintained until the charge was completed. In the CV charge phase, the diminishing charge current reduced the *iR*-drop effect. Consequently, we can observe the voltage decrease of cell nos. 3 and 8 in Fig. 10. However, the real voltage of these cells still increased in the meanwhile. Since the total voltage of 10 cells was fixed at 39.5 V in the CV charge phase, the voltage of cell no. 6 rose correspondingly with charging. The dispersion of the upper voltage at the end of the charge among these 10 cells

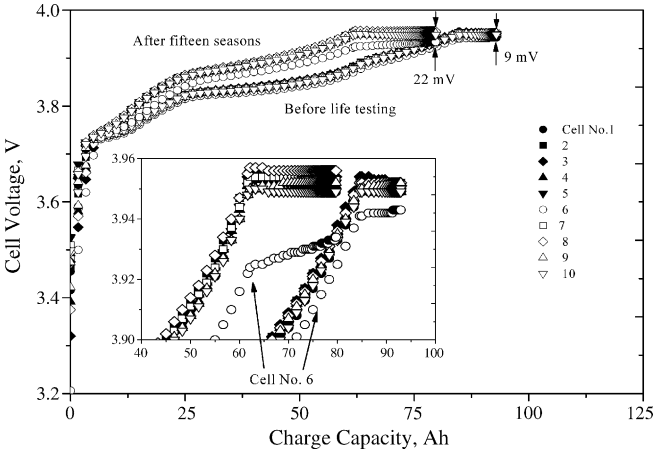

Fig. 10. Charge curves of capacity verification.

increased from the initial 9 mV to 22 mV after 15 seasons. We believe that the low discharge capacity of cell no. 6 was due to the upper voltage in the charge phase being much lower than in the other cells, which resulted in a serious charge capacity deficiency. In practical operation, we can use shunt circuit to adjust the each cell voltage at the end of charge prior to eclipse period, and hence suppress the detrimental influence of cell-capacity unbalance.

4. Conclusions

We are conducting cycle-life testing of a 100-Ah class lithium-ion battery in real-time testing at JAXA, simulating a GEO operation. 810 cycles have presently been completed, corresponding to 18 eclipse seasons. We raised the taper voltage after the 15th eclipse season to increase cell capacity.

The present data lead us to conclude that this battery operates well and meets the general requirements for a GEO mission, providing high voltage retention at the end of the discharge, small cell-voltage dispersion, low cell temperature, and good thermal distribution.

These promising test results suggest that this battery can reasonably be expected to work normally for storing power on a GEO mission.

Acknowledgements

The authors would like to acknowledge Mitsubishi Electric Corporation (MELCO) and GS Yuasa Technology Ltd. (GYT) for their supply of the battery and helpful discussions. Special thanks are also due to the technical staffs from Ryoei Technica Corporation for their support.

References

[1] Y. Sone, X. Wang, H. Kusawake, S. Kuwajima, Proceedings of the 2002 NASA Aerospace Battery Workshop, Marshall Space Flight Center, Huntsville, USA, 2002 (CD-ROM Version).
[2] X. Wang, Y. Sone, S. Kuwajima, J. Electrochem. Soc. 151 (2004) A273.
[3] X. Wang, C. Yamada, H. Naito, S. Kuwajima, J. Power Sources 140 (2005) 129.
[4] M. Goto, T. Gonai, T. Iwamoto, T. Inoue, K. Komada, Proceedings of the Seventh European Space Power Conference, ESA, Stresa, Italy, 2005 (CD-ROM Version).
[5] T. Kiyokawa, H. Yamazaki, M. Goto, T. Gonai, Proceedings of the 2002 NASA Aerospace Battery Workshop, Marshall Space Flight Center, Huntsville, USA, 2002 (CD-ROM Version).
[6] T. Gonai, T. Kiyokawa, H. Yamazaki, M. Goto, Proceedings of the 25th International Telecommunications Energy Conference, IEICE and the IEEE Power Electronics Society, Yokohama, Japan, 2003, pp. 234–240.
[7] N. Miyanaga, T. Inoue, H. Yoshida, K. Komada, T. Gonai, Proceedings of the 25th International Telecommunications Energy Conference, IEICE and the IEEE Power Electronics Society, Yokohama, Japan, 2003, pp. 234–240.
[8] T. Inoue, N. Imamura, H. Yoshida, M. Mizutani, Proceedings of the 2002 NASA Aerospace Battery Workshop, Marshall Space Flight Center, Huntsville, USA, 2002 (CD-ROM Version).
[9] J. Semerie, G. Dudley, J. Hausser, Proceedings of the Seventh European Space Power Conference, ESA, Stresa, Italy, 2005 (CD-ROM Version).

[10] R. Gitzendanner, E. Jones, C. Deroy, D. Carmen, Proceedings of the Seventh European Space Power Conference, ESA, Stresa, Italy, 2005 (CD-ROM Version).
[11] A. Bennetti, R. Spurrett, C. Thwaite, N. Russel, Proceedings of the Seventh European Space Power Conference, ESA, Stresa, Italy, 2005 (CD-ROM Version).
[12] R. Bugga, M. Smart, L. Whitcanack, J. Knight, R. Ewell, R. Surampudi, Proceedings of the 2002 NASA Aerospace Battery Workshop, Marshall Space Flight Center, Huntsville, USA, 2002 (CD-ROM Version).
[13] H. Yoshida, N. Imamura, T. Inoue, K. Komada, Electrochemistry 71 (2003) 1018.